Towards a gauge invariant method for molecular chiroptical properties in TDDFT

Daniele Varsano,*[ad] Leonardo A. Espinosa-Leal,[bd] Xavier Andrade,[bd] Miguel A. L. Marques,[cd] Rosa di Felice[a] and Angel Rubio[bd]

Received 16th February 2009, Accepted 17th March 2009
First published as an Advance Article on the web 14th April 2009
DOI: 10.1039/b903200b

We present an efficient scheme to calculate the chiroptical response of molecular systems within time dependent density functional theory using either a real-time propagation or a frequency-dependent Sternheimer method. The scheme avoids the commonly used sum over empty orbitals and has a very favorable scaling with system size. Moreover, the method is general and can be easily implemented. In the present work, we implemented it using a real-space pseudo-potential representation of the wave-functions and Hamiltonian. The specific use of non-local pseudo-potentials implies that a gauge correction term in the angular momentum operator must be included to ensure that the total scheme is fully gauge invariant. Applications to small organic chiral molecules are shown and discussed, addressing some deficiencies of present exchange–correlation functionals to describe the absolute position of the excitations. However, the shape or sign of the dichroism spectra comes out in excellent agreement with available experiments.

I. Introduction

Certain materials have the property of rotating linearly polarized light. This effect is usually referred to as optical activity, and forms the basis of one of the most useful spectroscopic techniques in chemistry, biology and materials science: circular dichroism. In the simplest version of this technique, one probes either the optical rotatory dispersion (ORD) or the electronic circular dichroism (ECD). The former approach consists of the measurement of the change in the angle of polarisation of the incident linearly polarised light as a function of the wavelength. In ECD measurements, alternatively, the target signal is the difference in absorption between right and left circularly polarised light, which induces an elliptical polarization as light travels through the medium. Molecular chirality (left and right handedness) is then directly probed. Chirality in general constitutes an area of great scientific and commercial interest: pharmaceutical science depends largely on chiral recognition, as well as catalysis in chemical industry and liquid crystal displays, among others.

Enantiomers, chiral molecules, play a fundamental role in the activity of living organisms (for example, sugars are right-handed and amino-acids are left-handed) and pharmaceutical complexes (*e.g.*, thalidomide, in its *R*-species, is effective against morning headaches in pregnant women but the *S*-enantiomer produces fetal deformations), and therefore the determination (and control) of the absolute configuration of chiral molecules is of paramount importance. For example, ECD in the ultraviolet is used to determine protein secondary structures[1] and the helical structure of nucleic acids[2] *in vacuo*. This powerful and sensitive spectroscopic tool can be extended beyond chiral molecules by placing the target molecule in a magnetic field so that it becomes optically active. This technique is known as magneto-chiral dichroism or magnetic circular dichroism (MCD).

Therefore, it was recognised early that the formulation and implementation of an efficient and predictive theoretical scheme to address chiroptical properties in different molecular systems would be instrumental in important fields of science. In fact, experimental spectra are often hard to interpret, and their comparison to theoretical models becomes essential to unveil the relevant structural and dynamical information. It is not surprising, therefore, that a considerable amount of effort has been devoted in the past decades to the development of such theoretical schemes.[3–5]

Following the seminal works by Rosenfeld and Condon,[6,7] several calculations of circular dichroism have been presented in different theoretical frameworks such as Hartree–Fock,[8,9] coupled cluster theory[10–15] and configuration interaction methods,[16] ground state density functional theory (DFT)[17] and time-dependent DFT (TDDFT).[18]

In the present work we follow an alternative TDDFT approach based on two different methods: real-time propagation and Sternheimer linear response. Performing real-time propagation is routinely done nowadays for linear and non-linear response properties[19–22] and was extended to ECD in ref. 23. Sternheimer linear response[24] is the standard technique for vibrational properties in the condensed matter physics community[25] (where it is known as density functional

[a] *National Center on Nanostructures and Biosystems at Surfaces (S3) of INFM-CNR, c/o Dipartimento di Fisica, Universitá di Modena e Reggio Emilia, Via Campi 213/A, 41100, Modena, Italy. E-mail: daniele.varsano@unimore.it*
[b] *Nano-Bio Spectroscopy group, Dpto. de Física de Materiales, Universidad del País Vasco UPV/EHU, Centro Mixto CSIC-UPV/EHU and DIPC, Av. Tolosa 72, San Sebastián, E-20018, Spain*
[c] *Université Claude Bernard Lyon I, CNRS UMR 5586, 69622, Villeurbanne, France*
[d] *European Theoretical Spectroscopy Facility (ETSF), E. U.*

perturbation theory) but it has also been applied to optical linear and non-linear response.[26] These methods have been successful in determining optical properties where only the electric field component of the light is relevant. However, dichroism is a mixed magneto-optical response, so the magnetic component of the light also has to be taken into account. Even though the formulation of quantum mechanics (or TDDFT) under magnetic fields is gauge invariant, this invariance might not be satisfied by approximate solutions of the corresponding equations.[27]

In this article we build upon the work of Yabana and Bertsch,[23] and present a formulation of dichroism that is fully gauge-invariant. We show that the enforcement of gauge invariance is fundamental to get a reliable description of the molecular dichroic response. Furthermore, we implemented several techniques, such as filtering of the pseudo potentials, that greatly improve the numerical efficiency of the scheme. We then apply this approach to a variety of benchmark systems where gas phase experiments are available. In particular, we compare calculated ECD spectra for three alkene compounds and both ECD and ORD for the methyloxirane molecule.

The article is organized as follows: in sect. II we describe the method and the implementation for the calculation of ECD (and MCD). In sect. III, the most important details of the numerical implementation are discussed. In sect. IV, the results for selected molecules are shown and compared with experimental results. Finally, in sect. V, we draw our conclusions and outline some perspectives for future studies.

II. Theoretical background

Real-time quantum mechanics is an alternative approach to standard frequency-dependent perturbation theory to calculate the system response under external perturbations. In this approach, the wave-function, or the single particle orbitals and the density in the TDDFT case, are propagated in time under a general time-dependent electromagnetic potential starting from a given initial state.

In this section, we present the derivation of a real-time formalism for the circular dichroic response in molecular systems. This derivation is analogous to the one used to obtain the polarizability, which was applied to the calculation of optical absorption spectra in real-time TDDFT.[19] We then show how, starting from the real-time expression, we can obtain in the frequency domain both the expression for the Sternheimer linear response perturbation theory and the canonical formula for the sum over states.[7]

A Optical activity in real-time

Chiroptical effects are based on the fact that some molecules interact differently with right (R)- and left (L)- circularly polarized light, so that the medium effectively has two refraction indexes, n_R and n_L. Dichroism can be quantified by the difference between the two refraction indexes, $\Delta n = n_L - n_R$. Physically, the real part of Δn measures the rotation of the polarization vector of an incident linearly polarized field (ORD), whereas the imaginary part accounts for the difference in the absorption (ECD).

Studying the interaction of an individual chiral molecule with a monochromatic electric and magnetic field starts with the linear equations for the induced electric ($\boldsymbol{p}(t)$) and magnetic ($\boldsymbol{m}(t)$) moments in terms of the external field (atomic units will be used throughout this paper, indexes j,k will be used for coordinates and p,q for energy levels)

$$p_j(t) = \sum_k \alpha_{jk} E_k(t) - \frac{1}{c}\sum_k \beta_{jk} \frac{\partial B_k(t)}{\partial t} \tag{2.1a}$$

$$m_j(t) = \sum_k \chi_{jk} B_k(t) + \frac{1}{c}\sum_k \beta_{jk} \frac{\partial E_k(t)}{\partial t}, \tag{2.1b}$$

where $\boldsymbol{\alpha}$ is the electric polarizability tensor, $\boldsymbol{\chi}$ the magnetic susceptibility and $\boldsymbol{\beta}$ the crossed response tensor in the time derivative of the fields.† By applying Maxwell equations in a medium that satisfies eqn (2.1) it is easy to prove that the isotropic average of $\boldsymbol{\beta}$,

$$\bar{\beta} = \frac{1}{3}\sum_j \beta_j, \tag{2.2}$$

is proportional to the difference between the refractive indexes for left and right polarized light‡

$$\Delta n = \frac{8\pi N\omega}{c}\bar{\beta}, \tag{2.3}$$

where N is the molecular density of the medium, and ω, the frequency.

The tensor $\boldsymbol{\beta}$ is therefore the key quantity that must be calculated in order to predict the ORD and the ECD spectra. In the case of response to a polychromatic electric field we have to define a frequency dependent tensor, $\boldsymbol{\beta}(\omega)$, so that eqn (2.1b), without considering an applied magnetic field, becomes

$$m_j(t) = -\frac{i}{c}\sum_k \int_{-\infty}^{\infty} \beta_{jk}(\omega)\omega E_k(\omega) e^{-i\omega t} d\omega. \tag{2.4}$$

Now, as a particular case we consider an electric field with equal intensity, $\boldsymbol{\kappa}$, for all frequencies: $\boldsymbol{E}(\boldsymbol{r},\omega) = \boldsymbol{\kappa}/2\pi$ (in the time domain this corresponds to $\boldsymbol{E}(\boldsymbol{r},t) = \boldsymbol{\kappa}\delta(t)$, where $\boldsymbol{r}$ is the position vector). By introducing this expression in eqn (2.4) and performing an inverse half-Fourier transform (with an infinitesimal imaginary component δ in the frequency) we obtain that

$$\beta_{jk}(\omega) = \frac{ic}{\omega\kappa_j}\int_0^{\infty} m_k(t) e^{i(\omega+i\delta)t} dt \tag{2.5}$$

where δ is an infinitesimal positive quantity. From eqn (2.5) we see that $\boldsymbol{\beta}$ can be calculated from the time-resolved electrically induced magnetic moment. For a quantum mechanical system, the magnetization is given by the total angular momentum, so

$$\beta_{jk}(\omega) = \frac{i}{2\omega\kappa_j}\int_0^{\infty} [L_k(t) + g_s S_k(t)] e^{i(\omega+i\delta)t} dt, \tag{2.6}$$

† An additional term couples the induced electric dipole with the magnetic field and *vice versa*. This term is of higher order and we can safely neglect it in our formulation (see eqn (55) in ref. 7).

‡ This expression is obtained neglecting the electric field due to the neighboring molecules: for a medium with randomly distributed molecules we obtain: $\Delta n = \frac{8\pi N\omega}{c}\bar{\beta}\frac{n^2+2}{3}$ where n is the mean index of refraction.

where g_s is the electron g-factor and $\boldsymbol{L}(t)$ is the expectation value of the orbital angular momentum operator

$$L_j(t) = \langle\psi(t)|\hat{L}_j|\psi(t)\rangle. \tag{2.7}$$

Similarly the expectation value of the spin operator, $\hat{S}$, should be considered for a system with finite total spin. In the derivation that follows, and in the calculations performed in this work, we restrict ourselves to cases where the contribution of $\hat{S}$ is negligible. However, this term has to be taken into account for open-shell systems and for the case of magnetic circular dichroism.

From this general derivation we can now determine the rotational strength function

$$R(\omega) = \frac{3\omega}{\pi c}\mathrm{Im}\bar{\beta}(\omega), \tag{2.8}$$

which physically characterizes the magnitude of the ECD.

B Real-time TDDFT

The scheme described above can be easily implemented in real-time TDDFT. For each direction j, the perturbation is applied as a phase factor of the ground-state Kohn–Sham (KS) wave-functions $\psi(t = 0^+) = e^{i\kappa_j r_j}\psi_{gs}$. Next, the orbitals are evolved using the time-dependent KS equations

$$i\frac{\partial\psi_p(\boldsymbol{r},t)}{\partial t} = H[n]\psi_p(\boldsymbol{r},t) \tag{2.9a}$$

$$n(\boldsymbol{r},t) = \sum_p \psi_p^*(\boldsymbol{r},t)\psi_p(\boldsymbol{r},t), \tag{2.9b}$$

calculating for each time the expectation value of the angular momentum

$$\boldsymbol{L}(t) = -i\sum_p \int \mathrm{d}\boldsymbol{r}\psi_p(\boldsymbol{r},t)(\boldsymbol{r}\times\nabla)\psi_p(\boldsymbol{r},t). \tag{2.10}$$

Then the values of $\boldsymbol{L}(t)$ for the three directions are introduced in eqn (2.6) from which $\boldsymbol{\beta}(\omega)$ is obtained in the energy range of interest.

C Perturbation theory formulation

Because the previous derivation is not standard, we show here that we can readily recover the standard expression of ECD in perturbation theory from our previous result. For each direction, j, and up to first order in the applied field, the time-dependent wave-function can be written as the ground state wave-function $|\psi_0\rangle$ (with energy ε_0) plus a sum of frequency dependent variations $|\delta\psi_{0,j}(\omega)\rangle$:

$$|\psi(t)\rangle = e^{-i\varepsilon_0 t}|\psi_0\rangle + \frac{\kappa_j}{2\pi}\int_{-\infty}^{\infty}\mathrm{d}\omega e^{i(\omega-\varepsilon_0)t}|\delta\psi_{0,j}(\omega)\rangle. \tag{2.11}$$

Inserting eqn (2.11) into eqns (2.7) and (2.6) (but performing a full Fourier transform in time) we get:

$$\beta_{jk}(\omega) = \frac{i}{2\omega}[\langle\delta\psi_{0,j}(-\omega)|\,\hat{L}_k\,|\psi_0\rangle + \langle\psi_0|\,\hat{L}_k\,|\delta\psi_{0,j}(\omega)\rangle] \tag{2.12}$$

This expression can be directly calculated from the occupied states only, by using Sternheimer perturbation theory (see section 2D below). However, if we now expand $|\delta\psi_{0,j}(\pm\omega)\rangle$ as a sum over states we recover the commonly used expression for the rotatory strength function:[28]

$$\beta_{jk}(\omega) = -\frac{i}{2\omega}\sum_p \langle\psi_0|\,\hat{r}_j\,|\psi_p\rangle\langle\psi_p|\,\hat{L}_k\,|\psi_0\rangle \times\left[\frac{1}{\varepsilon_p-\varepsilon_0+\omega-i\delta}-\frac{1}{\varepsilon_p-\varepsilon_0-\omega+i\delta}\right]. \tag{2.13}$$

Note that in eqn (2.13) both the electric and magnetic perturbations are treated on the same footing, while in our formalism of sections 2A and 2B there is a clear distinction: the electric field is applied as the perturbation and the magnetic dipole is the quantity that is calculated during the propagation. However, the two formalisms are not in contrast. In fact, we could alternatively obtain $\boldsymbol{\beta}$ from eqn (2.1a) instead of eqn (2.1b), namely applying the magnetic field as the perturbation and calculating the electric dipole. This procedure would involve a time-dependent magnetic field with a consequent complication of the formalism and of the numerical implementation.

D Sternheimer TDDFT

The circular dichroic response can also be computed in the Sternheimer linear response formalism. The main quantities in this scheme are the variations of the KS orbitals $\langle\psi_k(\omega)\rangle$ under an external perturbation, in this case a monochromatic electric field. They are obtained by solving the self-consistent set of linear equations

$$\{H[n]-\varepsilon_p\pm\omega\}\delta\psi_{n,j}(r,\omega) = -\delta H[\delta n_j]\psi_p(\boldsymbol{r}) \tag{2.14a}$$

$$\delta n_j(\boldsymbol{r},\omega) = \sum_p[\delta\psi_{n,j}^*(\boldsymbol{r},-\omega)\psi_p(\boldsymbol{r}) + \psi_p^*(\boldsymbol{r})\delta\psi_{n,j}(\boldsymbol{r},\omega)] \tag{2.14b}$$

(see ref. 26 for details). $\boldsymbol{\beta}$ can be then obtained from eqn (2.12). In contrast to some TDDFT implementations that directly use KS orbitals in eqn (2.13) neglecting all self-consistency effects in the response, both real-time and Sternheimer formulations include these effects and are in principle exact, provided that we know the exact exchange and correlation potential.

E Gauge-invariance

Molecular dichroism (either electric or magnetic) is an electromagnetic response. It can be viewed as the magnetic (electric) response of a molecule to an electric (magnetic) field. As such, we can expect that it will suffer from the same problems of gauge dependence as in the calculation of other magnetic responses, like magnetic susceptibilities or chemical shifts. In practical implementations, the gauge freedom in choosing the vector potential might lead to poor convergence with the quality of the discretization and to a dependence of the magnetic response on the origin of the simulation cell. In other words, an arbitrary translation of the molecule could introduce an unphysical change in the calculated observables. This broken gauge-invariance is well-known in molecular calculations with all-electron methods that make use of localized basis sets, such as Gaussians. The error can be traced

to the finite basis set representation of the wave-functions.[27]§ This problem is partially alleviated by working in the velocity gauge where the product of the dipole moment and angular momentum $\langle\psi_p|\nabla|\psi_q\rangle\langle\psi_p|\boldsymbol{r}\times\nabla|\psi_q\rangle$ does not change with any translation of the molecule, whereas the expression in the longitudinal gauge (as the one derived above) $\langle\psi_p|\boldsymbol{r}|\psi_q\rangle\langle\psi_p|\boldsymbol{r}\times\nabla|\psi_q\rangle$ depends on the origin if the basis set is not complete. A simple measure of the error is to check for the fulfillment of the hyper-virial relation,[32]

$$\langle\psi_p|\nabla|\psi_q\rangle = (\varepsilon_q-\varepsilon_p)\langle\psi_p|\boldsymbol{r}|\psi_q\rangle. \quad (2.15)$$

When working with a real-space mesh as in our case, this problem also appears, though milder, because the standard operator representation in the grid is not gauge-invariant. However, in this case it can be easily controlled by reducing the spacing of the mesh.

On the other hand, these methods typically require the use of the pseudo-potential approximation, where the electron–ion interaction is described by a non-local potential $V_{\rm nl}(\boldsymbol{r},\boldsymbol{r}')$. The advantage of using pseudo-potentials is clear as they eliminate the typically inert core electrons, reducing the computational cost of any *ab initio* electronic structure and excited-state calculations. For many electronic properties this substitution works very well (*e.g.*, for total energies, optical responses, phonons, *etc*).[33] However, the non-local part of the pseudo-potential introduces a fundamental problem when describing the interaction with magnetic fields or vector potentials in general. To preserve gauge-invariance, this term must be adequately coupled to the external electromagnetic field, otherwise the results will (strongly) depend on the origin of the gauge. For example an extra term has to be included in hyper-virial expression

$$\langle\psi_p|\nabla|\psi_q\rangle = (\varepsilon_q-\varepsilon_p)\langle\psi_p|\boldsymbol{r}|\psi_q\rangle + \langle\psi_p|[\boldsymbol{r},V_{\rm nl}]|\psi_q\rangle. \quad (2.16)$$

In general, the gauge-invariant non-local potential is given by

$$\langle\boldsymbol{r}|\hat{V}^{\boldsymbol{A}}_{nl}|\boldsymbol{r}\rangle = V_{\rm nl}e^{\frac{i}{c}\int_{\boldsymbol{r}}^{\boldsymbol{r}'}\boldsymbol{A}(x,t)\mathrm{d}x} \quad (2.17)$$

where $\boldsymbol{A}$ is the vector potential related to the applied magnetic field. For the case of a magnetic field there are two approaches to include this term,[34,35] the main difference between them relying on how the path integration in eqn (2.17) is performed.¶ For the case of chiroptical response, only first order corrections must be considered and we have not found significant differences between the results of the two schemes: thus, we used the scheme by Pickard and Mauri[35] for all the calculations presented in this work.

To illustrate the above discussion we show in Fig. 1 results for the ECD signal of *R*-methyloxirane. We performed two calculations of the ECD signal first for the molecule centered with respect to the origin of the simulation box, and then with the molecule displaced by 8 Å. We plot in Fig. 1 the difference between the two spectra both with and without the gauge correction. It is clear that the inclusion of the gauge term of eqn (2.17) eliminates the unphysical dependence of the ECD signal on the origin of the gauge; this is essential for reliable results.

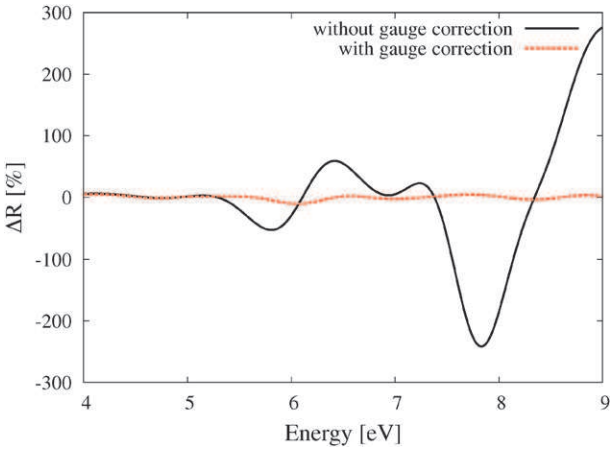

Fig. 1 Gauge-invariance test. Percentage difference in the rotatory strength function between two calculations performed with the molecule in the origin and displaced from the origin by 8 Å, without (solid black) and with (dashed red) the inclusion of the gauge correction from ref. 35. The system is *R*-methyloxirane. (The difference has been divided by the maximum of the signal: 0.004 Å^3.)

F Numerical properties

We note that both the real-time and Sternheimer approaches require only the calculation of the occupied Kohn–Sham orbitals and have a favorable scaling with the size of the system (quadratic for real-time propagation and cubic for Sternheimer linear response). With respect to other methods to calculate dichroic response, the cost is similar to the TDDFT method of ref. 18, but implementations based on eqn (2.13) are expected to exhibit a worse scaling with the number of atoms and the active-space considered in the wave-function expansion.

An additional advantage of the real-time approach is that it can be easily parallelized by distributing the orbitals among processors.[36] Since the propagation of each orbital is almost independent from the others, very little communication is required, resulting in a very efficient parallel scheme.

From a practical point of view, the relative numerical cost of the two methods we have presented depends on the information that one wants to gain. For the calculation of the response in the full spectral range, the real-time method is more efficient because the full spectrum can be obtained from a single run per perturbation direction. On the other hand, if the response for a small number of frequencies is desired, the Sternheimer formalism allows one to obtain the optical signals at few discrete frequencies with less computational cost.

§ Several techniques have been proposed over the past decades to solve the issue of the gauge dependence, such as the gauge including atomic orbital[29] (GIAO) or the individual gauge for localized orbitals[30,31] (IGLO) methods.

¶ Ismail-Beigi *et al.*[34] proposed to evaluate it by following a straight line from $\boldsymbol{r}$ to $\boldsymbol{r}'$. In our case it translates to changing the operator $\boldsymbol{r}\times\nabla$ in eqn (2.10) by $\boldsymbol{r}\times\nabla + \sum_{\boldsymbol{R}}\boldsymbol{r}\times[\boldsymbol{r},V^{\boldsymbol{R}}_{\rm nl}]$. The proposal by Pickard and Mauri[35] consists of using a path that passes through the coordinates of the atoms, so the operator that has to be followed during the evolution is: $\boldsymbol{r}\times\nabla + \sum_{\boldsymbol{R}}\boldsymbol{R}\times[\boldsymbol{r},V^{\boldsymbol{R}}_{\rm nl}]$, where $\boldsymbol{R}$ denotes the coordinates of the atoms.

III. Implementation

The two TDDFT formalisms described above, real-time and Sternheimer, were implemented in the code octopus.[36,37] In octopus, a real-space grid is used to represent the orbitals and other functions. The Troullier–Martins[38] norm-conserving pseudo-potential approximation is used to model the electron–ion interaction.‖ Unless otherwise stated, the exchange and correlation are treated at the level of the local density approximation (LDA) in the Perdew–Zunger parameterization.[39] The use of the usual GGA corrections does not significantly change the results discussed below.

Real space grids are advantageous for response calculations since the discretization error can be systematically controlled by increasing the size of the simulation box and reducing the grid spacing. We have checked that, with the parameters used in our calculations, the relation (2.16) is satisfied up to an error of 10^{-7}. A problem of real-space grid representations, however, is the spurious dependence of the total energy and other quantities on the relative position between ions and grid points, which breaks the translational invariance (see inset of Fig. 2). This artificial dependence is ascribed to the aliasing caused by Fourier components of the ionic potentials that have a higher frequency than the highest frequency resolved by the finite grid spacing. This problem has been extensively studied in the past[40] and can be considerably reduced by filtering the ionic potentials to eliminate these high Fourier components. For this purpose, we use the mask function filter of Tafipolsky and Schmid.[41] We show in Fig. 2 the effect of the high-frequency filtering. We find that the use of the filtering technique is crucial for efficient chiroptical response calculations: the plot in Fig. 2 in fact illustrates the error resulting in the difference dichroic signal when the molecule is displaced with respect to the computational grid (black line), which is removed by the frequency filter (red line). Note that the expectation value of the angular momentum operator is very sensitive to the position of the ions with respect to the grid points and this strong dependence gives rise to a significant ambiguity in the position, sign and intensity of the spectral peaks.

IV. Results and discussion

We now apply the method described in the previous sections to study the optical activity of some representative chiral molecules. The two approaches that we have introduced are used for distinct purposes. For the calculation of ECD spectra, related to the imaginary part of $\bar{\beta}$, the two methods give equivalent results but we show the output of the time-propagation, which is computationally more efficient than the Sternheimer approach. For the real part of $\bar{\beta}$, related to the ORD, we used the Sternheimer approach, because time-propagation results lack the required numerical precision.**

‖ For all the components the pseudo-potentials cutoff radii are 1.25 a.u. for hydrogen atoms, 1.47 a.u. for carbon atoms, and 1.39 a.u. for oxygen atoms.

** The real part as obtained from a direct Fourier transform of the angular momentum is very unstable below the first excitation. This was also observed in ref. 19 where a Kramers–Kroning transformation of the imaginary part was used to get the real part.

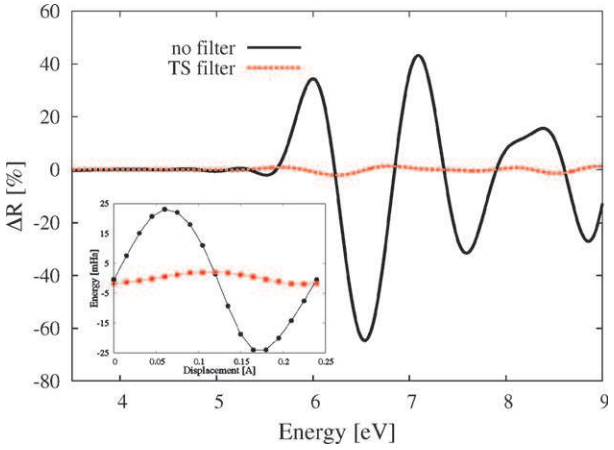

Fig. 2 Percentage difference in the rotatory strength function of *R*-methyloxirane between two calculations in which the molecule is displaced by 0.06 Å, without (solid black) and with (dashed red) pseudo-potential filtering[41]. Inset: deviation of the total energy from the average value, calculated for different displacements of the center of the molecule with respect to the grid origin, with (square red) and without (circle black) the filtering. The spacing of the grid is 0.24 Å.

For all systems we used the same set of simulation parameters that ensure a proper convergence of the results.†† We have observed that, with respect to total energy and even optical absorption calculations, more strict parameters are required for a proper convergence of the results, especially with respect to the volume of the simulation cell.

A (*R*,*S*)-methyloxirane

We have chosen as a first test case the enantiomeric species methyloxirane (also known as propylene oxide). Methyloxirane is one of the most typical benchmarks for optical activity calculations and it has been extensively studied in the past with different *ab initio* techniques.[10,42] The structure of *R*-methyloxirane was taken from ref. 43, where it was optimized at the SCF level using a 4-31G* basis-set and considering all degrees of freedom, with the exception of the C–H bond length.‡‡

The absorption and ECD spectra calculated in the time-propagation scheme are shown in Fig. 3. The spectra show the correct features expected for two enantiomeric species, *i.e.* an identical absorption spectrum (top panel) and ECD spectra with opposite signs at each frequency. When compared with experimental results (center panel in Fig. 3) the calculations present the correct shape and the correct sign in the ECD. The spectral positions of the peaks are underestimated by about 1.0 eV relatively to the experimental data. This underestimation of the lowest excitation energies has already been discussed (see, for example, ref. 10 and 18) and can probably

†† The grid was constructed considering overlapping spheres with a radius of 8.0 Å centered around each atom with a grid spacing of 0.20 Å. For the time-propagation scheme, a Lanczos exponential method was used with a time step of 0.02 $\hbar$ eV^{-1} and a total time of 24 $\hbar$eV.

‡‡ This structure was adopted so that our results are exactly comparable to the theoretical data. However, we also computed the optical spectra for a structure relaxed at the (B3LYP/cc-pVTZ) level, obtaining no significant deviations relative to the results shown in Fig. 3.

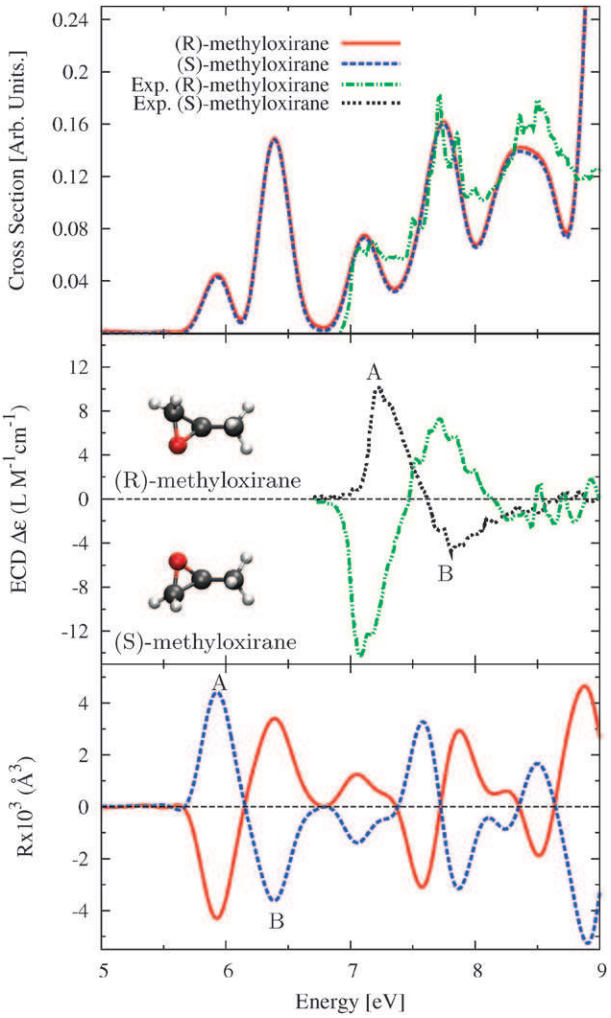

Fig. 3 Top panel: calculated absorption spectrum for *R*- (red solid) and *S*- (blue dotted) methyloxirane. For comparison, the experimental results[43] (green dashed-dotted) are given. Center panel: experimental results for the ECD of *R,S*-methyloxirane species (green-dotted-dashed and black-dotted respectively) reproduced from ref. 43. Bottom panel: calculated ECD of *R,S*-methyloxirane species (red solid and blue dotted lines, respectively). The results obtained with the Sternheimer equation are indistinguishable from those reported here from time-dependent propagation.

be ascribed to the approximation in the exchange and correlation functional (see discussion in section 4B).

The real part of $\boldsymbol{\beta}$ was studied using the Sternheimer scheme for an energy range between 0 and 4 eV. The results are detailed in Fig. 4, along with some reference theoretical and experimental data. In this case we have also studied the impact on the optical results of the use of different exchange–correlation functionals in the ground state calculations. In particular, we have determined the ground state of the molecule by using two different functionals, namely LDA and KLI.[44,45] The adiabatic LDA kernel was used in both cases to take into account the exchange and correlation effects in the response. We can see in Fig. 4 that our calculations agree in shape and order of magnitude with the reference calculations and experimental results. The KLI/ALDA approximation is in agreement with the experimental value

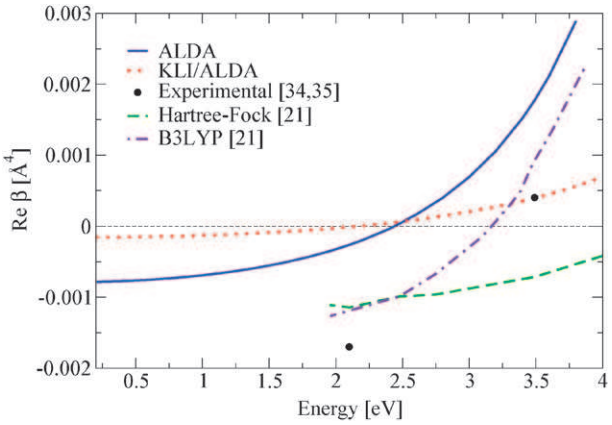

Fig. 4 Calculated $\Re e[\overline{\boldsymbol{\beta}}(\omega)]$ for (*S*)-methyloxirane using two different exchange and correlation potentials, LDA (solid blue) and KLI (dotted red), for the ground state Hamiltonian (in both cases the adiabatic LDA kernel was used for the response). For comparison, experimental values at 2.1[47] and 3.49 eV[48] (black dots), as well as Hartree–Fock (green-dashed) and B3LYP (indigo dashed-dotted)[49] computed data, are given.

at 3.49 eV but this is not the case at 2.1 eV where B3LYP and Hartree–Fock calculations seem to perform better, mainly due to the larger gap.[46]

B Alkenes: *trans*-cyclooctene, β-pinene and α-pinene

In this section we present the calculated ECD spectra for three different alkene molecules: *trans*-cyclooctene, β-pinene and α-pinene. These molecules were chosen due to availability of gas-phase experimental data of ECD in a large range of frequencies (5–9 eV)§§ and of quantum-chemistry and TDDFT results. Hence, they constitute a valid benchmark to evaluate the performance of the computational scheme described in this article. The structures of the molecules are taken from the supporting information of ref. 50 and were obtained *via* Monte Carlo searching and subsequently relaxed using DFT at the B3LYP/6-31G* level.

The calculated rotatory strength functions are shown and compared with experimental data in Fig. 5–7. The most important bands that constitute the ECD spectra are indicated with capital letters. For all molecules studied here, the calculated rotational strength function presents a very good qualitative agreement for both the sign and the shape of the spectra. The experimental peaks are often due to a superposition of several electronic transitions, and for this reason the calculated spectra (bottom panels of Fig. 5–7) are shown for two values of broadening given by the parameter δ of eqn 2.5: the larger one (solid red) is adopted to simulate the bandwidth of the experiments,¶¶ the smaller one (dotted blue) is adopted to resolve the underlying excitations beneath each peak. Looking at the position of excitation energies, as in the

§§ Our calculations do not take into account the solvent, whereas most experiments are done in solution. Therefore, for a benchmark of our theory the existence of experimental gas-phase data is essential.

¶¶ Beside the superposition of different excitations that are not resolved in the experiment, the bandwidth is also determined by temperature and vibronic effects that are not taken into account in our work.

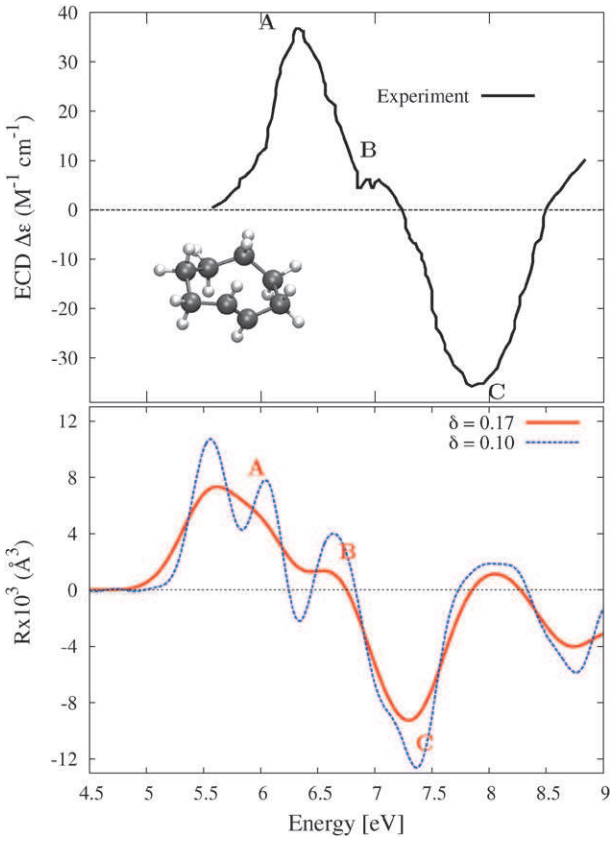

Fig. 5 Computed ECD spectrum of (*S*)-*trans*-cyclooctene (bottom) and experimental results for the same molecular species in the gas phase (top). The theoretical rotatory strength function (red-dashed, blue-dotted) was calculated for two different values of the broadening, as detailed in the legend. The experimental data are reproduced from ref. 51.

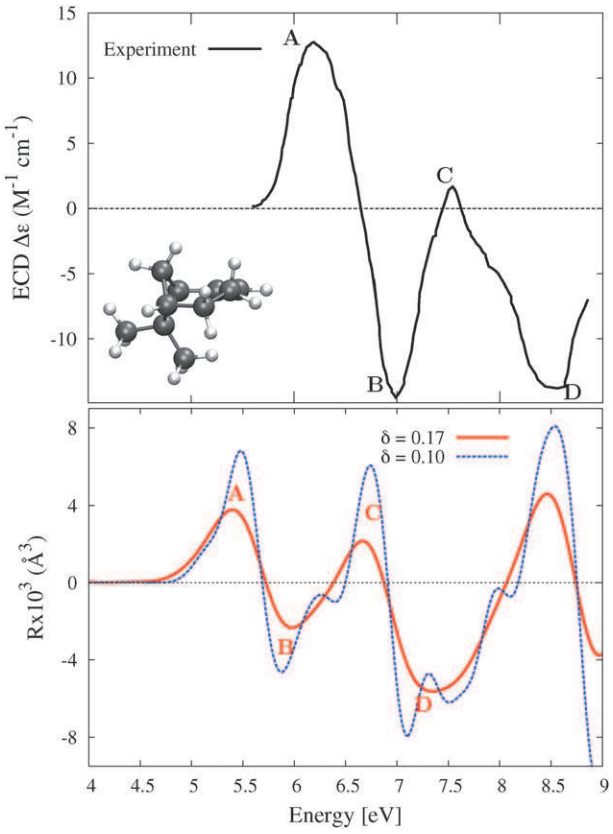

Fig. 6 Computed ECD spectrum of (1*S*,5*S*)-β-pinene (bottom) and experimental results for the same molecular species in the gas phase (top). The theoretical rotatory strength function (red-dashed, blue-dotted) was calculated for two different values of the broadening, as detailed in the legend. The experimental data are reproduced from ref. 51.

case of methyloxirane, we observe a systematic underestimation with respect to the experimental value ranging from 0.7 to 0.8 eV for the first peak, and a similar trend for the rest of the spectra. The effect of the ground state geometry on the ECD spectrum for these systems has been investigated in detail by McCann and Stephens,[50] concluding that it plays only a minor role. This discrepancy should therefore be ascribed to another source. The most probable origin is the approximation used for the exchange and correlation functional. McCann and Stephens[50] also showed that the excitation energies strongly depend on the functional used for these molecules, observing a systematic underestimation by 0.3–0.4 eV relative to experimental data when the B3LYP functional is used. The same effect is observed for α-pinene in ref. 52, where an underestimation by 0.53 and 0.33 eV is found using the BP86 and B3LYP functionals, respectively, while BHLYP and post Hartree–Fock methods (coupled cluster CC2 and multi-reference MP2) give overestimations of the frequencies of the peaks. It is not surprising that exchange–correlation effects also play a significant role in our work, considering, for example, that the lowest excitations of the alkene molecules present a large participation of Rydberg states that are not well described by the functional used in this work due to the lack of the $1/r$ tail in the potential. Indeed using a potential behaving as $1/r$, improved results may be obtained, yet not in quantitative agreement with experimental data. In our case what is somewhat remarkable is that, in spite of the fact that the spectra are shifted, the relative difference of excitation energies is well reproduced, as well as the relative intensities. Besides the systematic redshift of the peaks in the results of Fig. 5–7, our method reproduces well all the main experimental features for the studied molecules, even for the high-energy part of the spectrum.

In the case of the *trans*-cyclooctene molecule (Fig. 5) we obtain the main experimental features, namely the positive peak A, the shoulder B and the huge negative peak C. B and C are critical to reproduce in calculations. For instance, Diedrich and Grimme[53] were not able to reveal these fingerprints by a TDDFT calculation by using the sum over states of eqn (2.13) and the BHLYP hybrid functional. Instead, in the same reference they attained a very good agreement with the experimental results by using a multi-reference CI method.

Also for the β- and α-pinene (Fig. 6 and 7) we observe the correct sign and shape of the peaks. Our computed ECD spectrum for β-pinene is very similar to the results of a B3LYP calculation.[50] In the case of α-pinene, previous B3LYP[50,52] and CC2[52] results predict a huge positive and negative peak, respectively, around 7 eV, which is not present in the

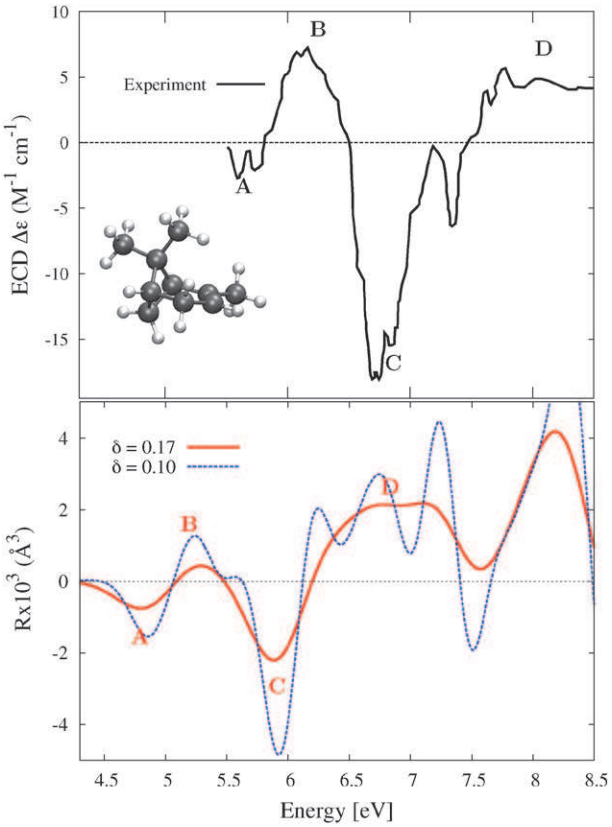

Fig. 7 Computed ECD spectrum of (1*R*,5*R*)-α-pinene (bottom) and experimental results for the same molecular species in the gas phase (top). The theoretical rotatory strength function (red-dashed, blue-dotted) was calculated for two different values of the broadening, as detailed in the legend. The experimental data are reproduced from ref. 51.

experimental data. Instead, we are able to reproduce the plateau at high energy (D), which becomes evident by using a broadening factor $\delta = 0.2$ eV. This better agreement can be explained by the several factors that differentiate our method from a sum over states formulation in a basis set representation: the systematic convergence of the discretization parameters which ensures that the electronic system will not be artificially constrained, the fact that the present method does not require unoccupied states and, finally, the inclusion of self-consistency effects of the Hartree, exchange and correlation kernels.

V. Conclusions

We have presented a general formalism for the study of the chiroptical properties of molecules. In our approach these properties are obtained by probing the magnetization of the system perturbed by an electric field. Special care has been taken to guarantee the gauge-invariance of the formalism and of the results. For this purpose, an extra term, related to the non-local pseudo-potential, must be added to the calculation of the magnetization. This correction term is independent of the representation and should be considered by any dichroic response approach that uses non-local potentials.

Based on this framework two different calculation strategies have been proposed. The first one is based on the real-time solution of the TDDFT Kohn–Sham equations and allows for the calculation of the whole dichroic spectra in a very efficient manner. The second one is based on the solution of the Sternheimer equation for the response to the external perturbation and allows direct calculation of both the chiroptical properties for a given frequency. The two strategies are complementary and allow to calculate real and imaginary part of the $\boldsymbol{\beta}$ tensor for a broad range of frequencies. However, the second strategy can be shown to be superior for the calculation of the real part of $\boldsymbol{\beta}$.

The results of calculations performed by us on benchmark molecules are in general agreement with experimental data and with the outcome of other TDDFT methods, especially looking at the shape of the spectrum. Clearly also an accurate prediction of excitation energies is needed to compute ECD spectra for molecules having a more complicated spectrum (overlapping bands with opposite signs). To this aim, a better description of the exchange and correlation functional is clearly required. Note, however, that our method is general and not restricted to any given functional.

It is straightforward to extend our framework to handle magnetic circular dichroism by performing ECD calculations under a magnetic field, analogous to what is done experimentally.[54] Other combined linear and non-linear electromagnetic responses could be studied as well. Another interesting extension would be the generalisation of the formalism for the treatment of periodic systems: this would allow the study of optical activity of crystalline systems or molecules in solvent or in the liquid phase.

Acknowledgements

We are grateful to S. Corni, A. Castro and M. Oliveira for stimulating discussions. This work was supported by the European Commission through Contracts N. FP6-029192 (IST FET-Open project DNA- NANODEVICES), e-I3 ETSF project (Contract Number 211956) and NANO-ERA CHEMISTRY, the Spanish MEC (FIS2007-65702-C02-01), "Grupos Consolidados UPV/EHU del Gobierno Vasco" (IT-319-07) and CSIC. M.A.L.M. acknowledges partial support from the Portuguese FCT through the project PTDC/FIS/73578/2006 and from the French ANR (ANR-08-CEXC8-008-01). We acknowledge CINECA CPU time granted through INFM-CNR, Barcelona Supercomputing Center, "Red Española de Supercomputacion" and SGIker ARINA (UPV/EHU).

References

1 B. A. Wallace, *J. Synchrotron Radiat.*, 2000, **7**, 289.
2 J. C. Sutherland, K. P. Griffin, P. C. Keck and P. Z. Takacs, *Proc. Natl. Acad. Sci. U. S. A.*, 1981, **78**, 4801.
3 R. D. Amos, *Chem. Phys. Lett.*, 1982, **87**, 23.
4 A. D. Buckingham, C. Graham and J. H. Williams, *Mol. Phys.*, 1983, **49**, 703.
5 R. D. Amos, N. C. Handy, K. J. Jalkanen and P. J. Stephens, *Chem. Phys. Lett.*, 1987, **133**, 21.
6 L. Rosenfeld, *Z. Phys.*, 1928, **52**, 161.
7 E. U. Condon, *Rev. Mod. Phys.*, 1937, **9**, 432.

8 P. L. Polavarapu, *Mol. Phys.*, 1997, **91**, 551.
9 P. L. Polavarapu and D. K. Chakraborty, *J. Am. Chem. Soc.*, 1998, **120**, 6160.
10 M. C. Tam, N. J. Russ and T. D. Crawford, *J. Chem. Phys.*, 2004, **121**, 3550.
11 J. Kongsted, T. B. Pedersen, M. Strange, A. Osted, A. E. Hansen, K. V. Mikkelsen, F. Pawlowski, P. Jorgensen and C. Hattig, *Chem. Phys. Lett.*, 2005, **401**, 385.
12 T. B. Pedersen, H. Koch, L. Boman and A. M. J. S. de Meŕs, *Chem. Phys. Lett.*, 2004, **393**, 319.
13 T. D. Crawford, *Theor. Chem. Acc.*, 2006, **115**, 227.
14 T. D. Crawford, M. C. Tam and M. L. Abrams, *J. Phys. Chem. A*, 2007, **111**, 12057.
15 T. D. Crawford and P. J. Stephens, *J. Phys. Chem. A*, 2008, **112**, 1339.
16 M. Pericou-Cayere, M. Rerat and A. Dargelo, *Chem. Phys.*, 1998, **226**, 297.
17 J. R. Cheeseman, M. J. Frisch, F. J. Devlin and P. J. Stephens, *J. Phys. Chem. A*, 2000, **104**, 1039.
18 J. Autschbach, T. Ziegler, S. J. A. van Gisbergen and E. J. Baerends, *J. Chem. Phys.*, 2002, **116**, 6930.
19 K. Yabana and G. F. Bertsch, *Phys. Rev. B*, 1996, **54**, 4484.
20 K. Yabana and G. F. Bertsch, *Int. J. Quantum Chem.*, 1999, **75**, 55.
21 G. F. Bertsch, J.-I. Iwata, A. Rubio and K. Yabana, *Phys. Rev. B*, 2000, **62**, 7998.
22 M. A. L. Marques, X. López, D. Varsano, A. Castro and A. Rubio, *Phys. Rev. Lett.*, 2003, **90**, 258101.
23 K. Yabana and G. F. Bertsch, *Phys. Rev. A*, 1999, **60**, 1271.
24 R. Sternheimer, *Phys. Rev.*, 1951, **84**, 244.
25 S. Baroni, S. de Gironcoli, A. Dal Corso and P. Giannozzi, *Rev. Mod. Phys.*, 2001, **73**, 515.
26 X. Andrade, S. Botti, M. A. L. Marques and A. Rubio, *J. Chem. Phys.*, 2007, **126**, 184106.
27 J. Gauss, in *Modern Methods and Algorithms of Quantum Chemistry*, ed. J. Grotendorst, John von Neumann Institute for Computing, Jülich, 2000, **vol. 3** of NIC series, pp. 541–592, 2nd edn, see section 3.4 and references therein.
28 A. E. Hansen and T. D. Bouman, *Adv. Chem. Phys.*, 1980, **44**, 545.
29 K. Wolinski, J. F. Hinton and P. Pulay, *J. Am. Chem. Soc.*, 1990, **112**, 8251.
30 W. Kutzelnigg, *Isr. J. Chem.*, 1980, **19**, 193.
31 M. Schindler and W. Kutzelnigg, *J. Chem. Phys.*, 1982, **76**, 1919.
32 T. D. Bouman and A. E. Hansen, *J. Chem. Phys.*, 1977, **66**, 3460.
33 E. Luppi, H.-C. Weissker, S. Bottaro, F. Sottile, V. Veniar, L. Reining and G. Onida, *Phys. Rev. B*, 2008, **78**, 245124.
34 S. Ismail-Beigi, E. K. Chang and S. G. Louie, *Phys. Rev. Lett.*, 2001, **87**, 087402.
35 C. J. Pickard and F. Mauri, *Phys. Rev. Lett.*, 2003, **91**, 196401.
36 A. Castro, M. A. L. Marques, H. Appel, M. Oliveira, C. A. Rozzi, X. Andrade, F. Lorenzen, E. K. U. Gross and A. Rubio, *Phys. Status Solidi B*, 2006, **243**, 2465.
37 M. A. L. Marques, A. Castro, G. F. Bertsch and A. Rubio, *Comput. Phys. Commun.*, 2003, **151**, 60.
38 N. Troullier and J. L. Martins, *Phys. Rev. B*, 1991, **43**, 1993.
39 J. Perdew and A. Zunger, *Phys. Rev. B*, 1981, **23**, 5048.
40 R. D. King-Smith, M. C. Payne and J. S. Lin, *Phys. Rev. B*, 1991, **44**, 13063.
41 M. Tafipolsky and R. Schmid, *J. Chem. Phys.*, 2006, **124**, 174102.
42 J. Kongsted, T. B. Pedersen, L. Jensen, A. E. Hansen and K. V. Mikkelsen, *J. Am. Chem. Soc.*, 2006, **128**, 976.
43 M. Carnell, S. D. Peyerimhoff, A. Breest, K. H. Godderz, P. Ochmann and J. Hormes, *Chem. Phys. Lett.*, 1991, **180**, 477.
44 J. B. Krieger, Y. Li and G. J. Iafrate, *Phys. Rev. A*, 1992, **45**, 101.
45 J. B. Krieger, Y. Li and G. J. Iafrate, *Phys. Rev. A*, 1992, **46**, 5453.
46 S. Kümmel and L. Kronik, *Rev. Mod. Phys.*, 2008, **80**, 3.
47 A. Rauk, *J. Am. Chem. Soc.*, 1981, **103**, 1023.
48 T. Muller, K. Wiberg and P. Vaccaro, *J. Phys. Chem. A*, 2000, **104**, 5959.
49 E. Giorgio, C. Rosini, R. Viglione and R. Zanasi, *Chem. Phys. Lett.*, 2003, **376**, 452.
50 D. M. McCann and P. J. Stephens, *J. Org. Chem.*, 2006, **71**, 6074.
51 M. G. Mason and O. Schnepp, *J. Chem. Phys.*, 1973, **59**, 1092.
52 C. Diedrich and S. Grimme, *J. Phys. Chem. A*, 2003, **107**, 2524.
53 S. Grimme and M. Waletzke, *J. Chem. Phys.*, 1999, **111**, 5645.
54 P. J. Stephens, *J. Chem. Phys.*, 1970, **52**, 4389.